High-Gain Circularly Polarized Fabry–Pérot Patch Array Antenna With Wideband Low-Radar-Cross-Section Property

QIANG CHEN AND HOU ZHANG

Air-Defense and Antimissile Institute, Air Force Engineering University, Xi'an 710051, China

Corresponding author: Qiang Chen (1062620145@qq.com)

ABSTRACT In this paper, we explore the adoption of a chessboard polarization conversion metasurface (CPCM) for constructing a low-radar-cross-section (RCS), high-gain circularly polarized patch array antenna. The proposed CPCM is used as the CPCMs' chessboard configuration, which consists of adjacent two-layer substrates that have three metallic models. Low RCS is achieved by 180° (±30°) reflection phase variations of two adjoining PCMSs. Gain enhancement is achieved by adopting a Fabry–Pérot cavity constituted by a PCM and the antenna's ground. The antenna with a CPCM that operates at X-/Ku-band, excited by the feeding network that is rotated sequentially, is measured and fabricated. The patch array antenna impedance bandwidth based on the PCM was measured as 3.3 GHz (9.5–12.8 GHz) with a 3-dB axial ratio bandwidth of 11.6% and a high gain of 13.4 dBiC (9.5–12 GHz), more than 2.5 dB higher when compared with a patch antenna without a PCM. In addition, the patch array antenna produced a useful wideband RCS decrease in the operational bandwidth from 9 to 13 GHz.

INDEX TERMS Low radar cross-section, dual patch, circularly polarized, polarization conversion metasurface.

I. INTRODUCTION

Metamaterials, containing electromagnetic band-gap structures, left-handed materials, metasurfaces, as well as frequency-selective surfaces, have been widely deployed as inartificially homogeneous or inhomogeneous electromagnetic structures owing to their unusual features [1], [2]. In particular, a vital adoption for polarization conversion (PC), namely two-dimensional (2D) metamaterial, can gain circularly polarized waves from linearly polarized waves [3], [4]. For example, using the metallic 2D metamaterial described in [5], a theoretical analysis for polarization rotation from the linearly polarized state to circularly polarized waves was conducted by Silveirinha. Nevertheless, because of the spatial 3D configuration's large size, the design would not be applicable to low-profile configurations. Currently, many planar 2D metamaterials (MSs) are designed for the purpose of realizing polarization rotation from a linear to a circularly polarized state [2], [6], [7]. Because of the twist structures gained through the rotation of the MS units, a majority of them can achieve the polarization change.

In this paper, a high-gain, low-radar-cross-section (RCS) antenna achieved by adopting a partially reflecting surface is put forward. The upper surface, which has resistors, can decrease the backward RCS under such a structure by adsorbing energy within the forthcoming electromagnetic (EM) waves [9], [10]. Nevertheless, fabricating the antenna has been rather difficult since many resistors, optimally, require welding. For the purpose of reducing the complexity of fabrication, we were able to adopt an AMC chessboard configuration instead [11].

Circularly polarized (CP) antennas with low RCS have recently attracted increasingly more attention for use in several stealth platforms because they mitigate the issue of polarization mismatch losses between receiving and transmitting antennas. In [12], metasurface absorbers as well as reconfigurable technologies were connected to achieve the low-RCS characteristics for a CP/linearly polarized (LP) antenna. Different from other technologies, in [13] the elements' random phase allocation was employed to introduce an antenna array with low-RCS CP. Nevertheless, the RCS reduction strategies for previous CP antenna designs have been limited for narrow-band operations.

Polarization conversion metasurfaces (PCMs) have been put forward within our primary studies for achieving broadband low-RCS antennas and designing low RCS

surfaces [14]–[16]. Compared with the RCS reduction strategies based on AMC [6], [11], PCM-based low-RCS surfaces are able to be designed by optimizing just a single element type rather than two. In addition, the maximum RCS reduction value, along with the RCS reduction band, has been made harmonious by just optimizing the polarization conversion ratio and the polarization conversion band separately [14]. Nevertheless, the in-band RCS was not decreased in [14] with the goal of avoiding degradation of antenna radiation performance.

To solve the above-mentioned issues, an original kind of high-gain, wideband, low-RCS, and CP antenna, conceived on the basis of chessboard polarization conversion metasurfaces (CPCMs), is advanced within this paper. A novel planar PCM structure, established on the basis of a three-layer MS, is used in this study to realize polarization conversion. Next, being an application, a patch array antenna that is covered by the proposed PCM structure was designed. High-gain, wideband, and low RCS were then achieved by the designed CP patch array antenna. The characteristics of a wideband low RCS were achieved through the reflected waves' phase cancellation from adjacent PCMs. Gain enhancement was achieved by adopting a Fabry–Pérot (FP) cavity and the broader axial ratio (AR) bandwidth achieved through advanced polarization purity. The resulting high-gain, wideband, low-RCS CP antenna is, to the best of our knowledge, reported here for the first time. Upon comparison with other studies, three specific contributions have emerged from this study: (1) wideband RCS reduction containing out-of- as well as in-band components; (2) CP antenna RCS reduction; and (3) a broader AR bandwidth in addition to gain enhancement. The remaining parts of this Letter are organized as follows. In Section II, we discuss the CPCM design methodology as well as its mechanism. In Section III, we introduce the antennas' measurements and its design with and without a CPCM; the scattering property and radiation features are also discussed. Conclusions are presented in Section IV.

II. CONFIGURATION AND ANALYSIS OF ANTENNA

Figure 1 shows the patch-feeding structure and the planar PC structure put forward recently based on AMC. In particular, the PCM consists of three layers. The bottom and top layers are comprised of an array arranged in a 4×4 layout by adopting a quasi-L-shaped metasurface cell with periodicity W that has been printed on the bottom and top sides of an FR4 substrate ($\tan\delta = 0.02$ and $\varepsilon_r = 4.4$). The middle layer has a square-ring metallic part. A traditional patch antenna is constituted to couple energy to the PCM structure. The feeding layers and PCM are separated by a FP cavity, in which gain enhancement is completed by the impact of FP resonance. Then, as displayed in Fig. 2, the array antenna will be constituted on the basis of the polarization conversion metasurfaces' chessboard configuration (PCM). Therefore, a low RCS will be achieved for the reflected waves' phase cancellation from the adjacent PCMs. The concepts of the parameters for all the functional layers are shown in
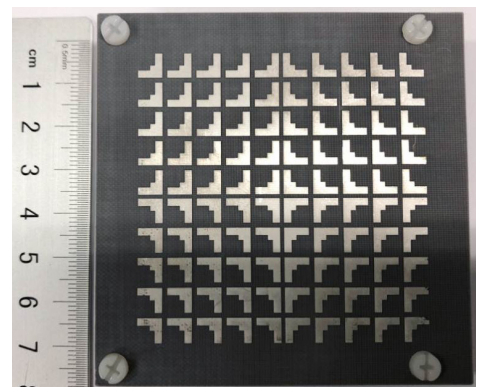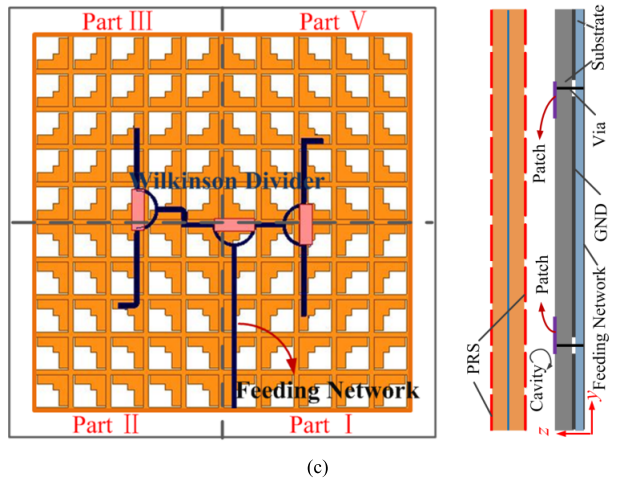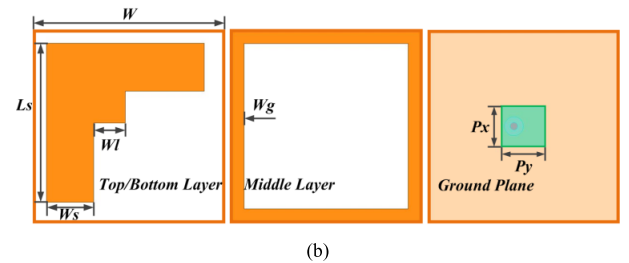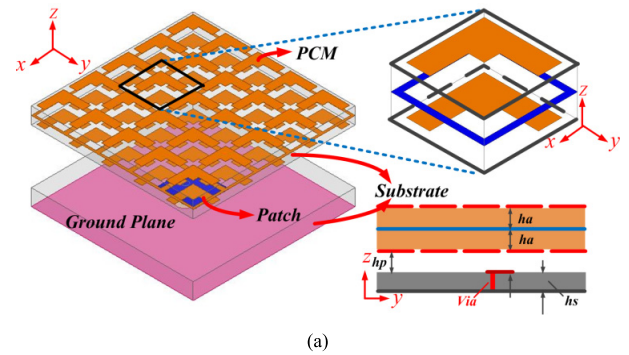

(a)

(b)

(c)

FIGURE 1. Topology of the PRRS unit with large PR bandwidth: (a) array antenna, (b) top view, (c) array antenna. Dimensions are $P_Y = 7.5$, $P_X = 6.1$, $W = 6$, $h_S = 3$, $W_a = 0.4$, $h_a = 1.524$, $W_l = 1$, $W = 5$, $G = 0.5$, $W_S = 1.5$, $L_S = 5$, and $h_P = 5.8$ (all in mm).

Fig. 1(a) and (b), and the optimized dimensions listed in the caption.

It is necessary to ensure that two prerequisites will result in a CP wave when a LP wave passes through a PCM [4].
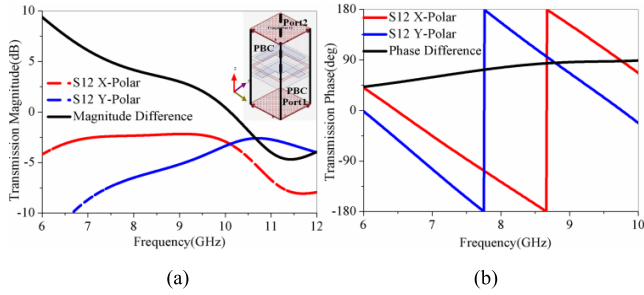
(a)   (b)

FIGURE 2. Coefficients of co- as well as cross-polarization transmission S12 X/Y-polar: (a) magnitude as well as magnitude difference and (b) phase as well as phase difference.
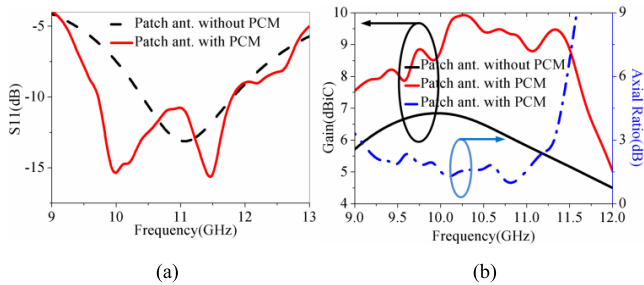

(a)   (b)

FIGURE 3. Simulated outcomes of the unit PRRS alone: (a) reflection coefficients and (b) total gain and AR.

First, the difference in phase between the cross-polarization component S12 X-polar and the co-polarization transmission coefficient S12 Y-polar is approximately 90° from 8 to 10 GHz [Fig. 2(b)]. Second, their difference in magnitude should not be larger than 3 dB [Fig. 2(a)]. The distance from right-hand circularly polarized (RHCP) antenna H to the PCM was 5.8 mm [Fig. 2(a)]. Figure 3 shows the simulation outcomes of the boresight RHCP/LP gain, the reflection coefficients, as well as the RHCP antennas' AR versus frequency results with or without PCM. It is noteworthy that the patch antenna's boresight RHCP gain with PCM in the impedance bandwidth from 9.5 to 12 GHz was higher compared with the LP gain of a standalone patch antenna. In addition, the RHCP antenna's AR with PCM was below 3 dB between 9 and 11.5 GHz. The simulated outcomes illustrate that PCMs are capable of converting a LP wave into a RHCP wave, which is dependent on the polarization conversion metasurfaces' transmission features in [17]. Moreover, the antenna's gain is developed as well, and the reason is given below.

As presented in Fig. 3, the outcomes of the comparisons with or without PCM are simulated just for unit structure, and it is clearly seen that both bandwidth and gain improvement are achieved with a PCM covering. Later, to schematically explain the mechanism to generate the CP radiation from a patch antenna for a LP state on the basis of a three-layer MS, which has some similarities with the interpretation in [9], an equivalent mode was provided, as presented in Fig. 2.

The RHCP antenna's gain enhancement with PCM was achieved by FP resonance impact. In accord with the design guideline in [4], the resonance condition of the circularly polarized FP (CPFP) cavity should meet the resonance requirements for y- and x- polarization components.
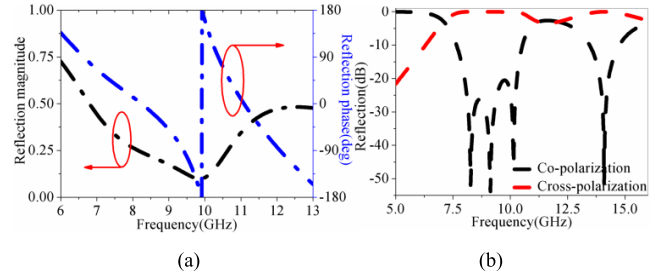

(a)   (b)

FIGURE 4. (a) x- and y-component simulated reflection magnitudes and phases and (b) simulated co- and PCM cross-polarization reflections.

As presented in [8], the PCM's reflection coefficients in the x and y directions should be in a similar condition for meeting the same resonance situation. In addition, the resonance cavity height (H) can be calculated by

$$H = \frac{c}{f}\left(\frac{\Phi_{1x} + \Phi_{2x} + 2n\pi}{4\pi}\right) = \frac{c}{f_0}\left(\frac{\Phi_{1y} + \Phi_{2y} + 2n\pi}{4\pi}\right), \quad (1)$$

where c is the speed of light in vacuum, H the height, and n an integer ($n = 0, 1, 2, \ldots$). Φ_{1x} and Φ_{1y} are the antenna ground's reflection coefficient phases in the x and y directions, respectively, and Φ_{2x} and Φ_{2y} the PCM's corresponding phases.

We assume that n for the two polarizations share the same value; Eq. (1) then indicates that

$$\Phi_{1x} + \Phi_{2x} = \Phi_{1y} + \Phi_{2y}, \quad (2)$$

which implies that it is necessary for the sum of the reflection-coefficient phases to be equal in two directions to meet the same resonance situation for the two polarizations. Moreover, the antenna ground's reflection-coefficient phases in the x and y directions are equal to π, which means that $\Phi_{1x} = \Phi_{1y} = \pi$. Thus, Φ_{2x} should be equal to Φ_{2y} if a high-gain CP antenna is expected to be achieved by adopting the FP resonance cavity requirement. Figure 5(a) presents the PCM's phases and simulated reflection-coefficient magnitudes. The same curve is shared by the reflection magnitudes in reflection phases and x and y directions, and is able to be interpreted through the symmetrical structure the same way as a +45° diagonal. The same curves for magnitudes and reflection phases illustrate that PCMs are capable of constructing the resonant CPFP cavity, which is illustrated in terms of radiation development in Fig. 4(b). The CPCM serves as the transmission structure so that it will be rather easy to analyze the backscattering characteristics of the antenna. The PCM's unit cell is simulated with the PEC ground. The PEC distance and the unit cell were optimized as 5.8 mm. Figure 4(b) presents the infinite PCM unit cell's cross- as well as co-polarization reflections backed with the PEC ground. It can be seen that the reflection coefficients' cross-polarization element turns out to be a main component, while the dominance of the co-polarization is lost from 6 to 15 GHz (expected from 12 to 13 GHz). The PCM's chessboard configuration is selected due to its wideband, low-RCS characteristics [14].

The RCS reduction capability relies on the CPCM's reflective features. As presented in Fig. 4(b), RHCP radiation was reached at the time the PCM was placed over the patch antenna [Fig. 2(b)]. Likewise, RHCP radiation can be collected by replacing the PCM with a mirror one. Considering the CPCM's arrangement, all the antenna factors under their corresponding PCM/mirror PCM arrangements should not be fed by in-phase excitation or planned in the same orientation. The supplement of RHCP and LHCP radiation from the surrounding PCMs will produce four grating lobes and create a gain-drop in the boresight direction if two types of PCMs have been excited by the orientation's RHCPs with similarities, which can be depicted by antenna array theory [18]. For the purpose of mitigating such types of interference, a RHCP antenna array with CP radiation on the basis of a feeding network that is rotated sequentially was selected as the source antenna. The feeding network that is rotated sequentially and can excite four orthogonal RHCPs was printed on the bottom surface of the substrate, which is 1 mm thick. The surrounding RHCPs were excited with a 90° phase difference as well as the same magnitude. Only the RHCP wave will be created when all the LP waves pass through the mirror PCM or the PCM. Therefore, gain degradation will not exist in the boresight direction. Nice scattering characteristics can be realized with no paucity of radiation features by adopting such a source. Considering the reference antenna's CP radiation performance, it seems unnecessary to create RHCP radiation using CPCM. Nevertheless, the antenna with CPCM possesses a broader AR bandwidth since greater polarization purity has been realized by replacing four LP factors by four CP factors. Moreover, RHCP gain can be developed at the operational frequency. Considering the scattering characteristics, wideband, low RCS can be achieved by adopting CPCM. Owing to the CPCM's symmetrical structure, there are some similarities in RCS reduction and *x*- and *y*-polarized incident waves. Therefore, scattering characteristics as well as radiation performance maintain a trade-off in the complementary design of the CPCM arrangement and the radiation source.
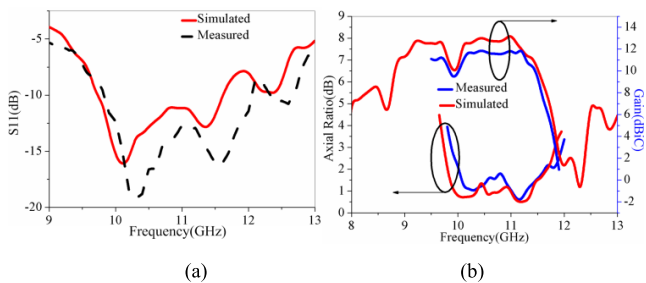

FIGURE 5. Measured and simulated outcomes of the suggested antenna (a) |*S*11| and (b) RHCP radiation gain and AR.

III. MEASUREMENT AND SIMULATION OUTCOMES

Finally, in accord with the developed structural parameters, the antenna prototype was generated and tested. As shown in Fig. 5(a) and (b), the proposed antenna has a measured 3-dB AR bandwidth of 3.5 GHz (9.5–13 GHz), an average
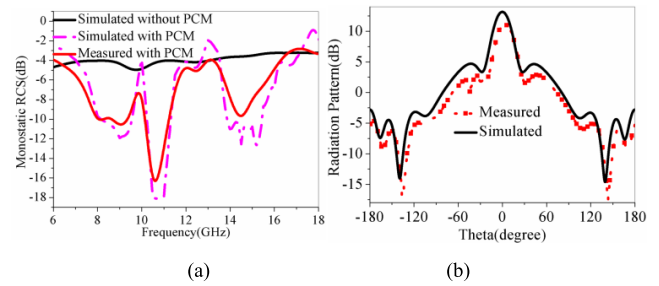

FIGURE 6. Simulated outcomes for the referenced CP and LP antennas. (a) *S*11 and (b) radiation gain and AR.
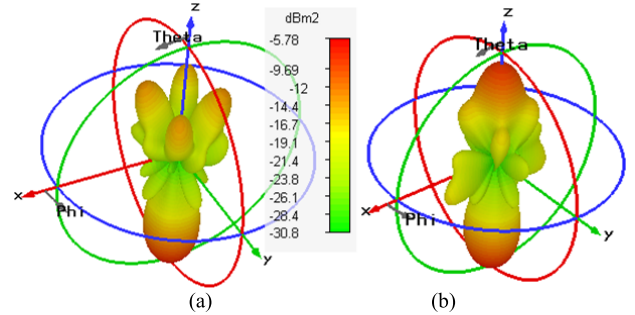

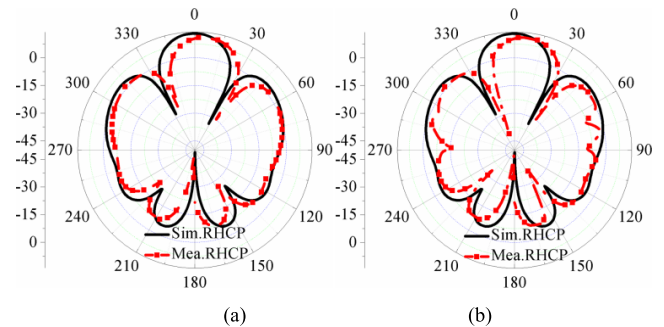**FIGURE 7.** 3D bistatic scattered field at 10.5 GHz in ordinary incidence for antenna (a) with and (b) without CPCM.

FIGURE 8. Radiation models of measured and simulated RHCP at 11.0 GHz in (a) *xoz* and (b) *yoz* planes.

RCS reduction of 7 dB, and a 10-dB bandwidth of 3.3 GHz (9.5–12.8 GHz), in correspondence with the PR band and in satisfactory agreement with the simulated outcomes as well. The |*S*11| parameters of the antenna were quantified with a vector network analyzer (Agilent Model E8361A). The RHCP, RHCP radiation models, and AR were calculated in an anechoic chamber by adopting a normal-gain horn antenna to be a reference and computed by adopting the information from their remote components with formulae from the literature [9].

In addition, as shown in Fig. 6(b), the peak RHCP radiation gain quantified on the *z* axis inside the AR band was 13.4 dB (gained at 11 GHz), with a degradation of 0.5 dB within the simulated results. Figure 7 shows both antennas' simulated 3D bistatic scattered field at 10.5 GHz in ordinary incidence. The energy in the ordinary aspect is again allocated within four grating lobes and the energy in the ordinary aspect is again allocated into four aspects (315°, 26°), (225°, 26°), (135°, 26°), and (45°, 26°). As shown in Fig. 8(a) and (b),

the proposed antenna yielded excellent broadside RHCP radiation with excellent cross-polarization under 25 dB in the CP operational bandwidth within the two planes. With a fundamental structure as well as good performance, the proposed antenna can be adopted for use in the X/Ku (10–13 GHz) bands.

IV. CONCLUSIONS

We have presented a low-RCS CP RHCP antenna with high gain and a wide bandwidth using an original polarization conversion in accordance with a three-layer PCM. Through necessary parametric research, numerical optimizations, and theoretical evaluation, the proposed dual-patch-based PCM antenna showed a 3-dB AR bandwidth of 3.5 GHz (9.5–13 GHz) and a simulated impedance bandwidth of 3.3 GHz (9.5–12.8 GHz), which were validated by measurements. The RCS of the novel antenna is lower than that of the reference antenna from 6 to 15 GHz (except for 12–13 GHz). Moreover, the proposed antenna shows a better AR property in the X band upon comparison with the results from current related works. It also created satisfactory RHCP with a peak broadside benefit of 13.4 dB. Because of its better AR features, the original antenna based on PCM has potential applications in the X/Ku band.

REFERENCES

[1] J. Zhu and G. V. Eleftheriades, "A compact transmission-line metamaterial antenna with extended bandwidth," *IEEE Antennas Wireless Propag. Lett.*, vol. 8, pp. 295–298, 2009.

[2] C. L. Holloway, E. F. Kuester, J. A. Gordon, J. F. O'Hara, J. Booth, and D. R. Smith, "An overview of the theory and applications of metasurfaces: The two-dimensional equivalents of metamaterials," *IEEE Antennas Propag. Mag.*, vol. 54, no. 2, pp. 10–35, Apr. 2012.

[3] B. Ratni, A. de Lustrac, S. Villers, and S. N. Burokur, "Low-profile circularly polarized Fabry–Perot cavity antenna," *Microw. Opt. Technol. Lett.*, vol. 58, no. 12, pp. 2957–2960, 2016.

[4] R. Orr, G. Goussetis, and V. Fusco, "Design method for circularly polarized Fabry-Perot cavity antennas," *IEEE Trans. Antennas Propag.*, vol. 62, no. 1, pp. 19–26, Jan. 2014.

[5] M. G. Silveirinha, "Design of linear-to-circular polarization transformers made of long densely packed metallic helices," *IEEE Trans. Antennas Propag.*, vol. 56, no. 2, pp. 390–401, Feb. 2008.

[6] Y. Jia, Y. Liu, and S. Gong, "Wideband high-gain circularly polarized planar antenna based on polarization rotator," in *Proc. Int. Conf. Electromagn. Adv. Appl. (ICEAA)*, Cairns, QLD, Australia, Sep. 2016, pp. 416–419.

[7] J. Y. Chin, M. Lu, and T. J. Cui, "Metamaterial polarizers by electric-field-coupled resonators," *Appl. Phys. Lett.*, vol. 93, no. 25, p. 251903, 2008.

[8] S. A. Muhammad, R. Sauleau, L. Le Coq, and H. Legay, "Self-generation of circular polarization using compact Fabry–Perot cavity antennas," *IEEE Antennas Wireless Propag. Lett*, vol. 10, pp. 907–910, Sep. 2011.

[9] L. Zhang and T. Dong, "Low RCS and high-gain CP microstrip antenna using SA-MS," *Electron. Lett.*, vol. 53, no. 6, pp. 375–376, Mar. 2017.

[10] K. Li, Y. Liu, Y. Jia, and Y. J. Guo, "A circularly polarized high-gain antenna with low RCS over a wideband using chessboard polarization conversion metasurfaces," *IEEE Trans. Antennas Propag.*, vol. 65, no. 8, pp. 4288–4292, Aug. 2017.

[11] Y. J. Zheng, J. Gao, X. Y. Cao, S. J. Li, and W. Q. Li, "Wideband RCS reduction and gain enhancement microstrip antenna using chessboard configuration superstrate," *Microw. Opt. Technol. Lett.*, vol. 57, no. 7, pp. 1738–1741, 2015.

[12] K. Kandasamy, B. Majumder, J. Mukherjee, and K. P. Ray, "Low-RCS and polarization-reconfigurable antenna using cross-slot-based metasurface," *IEEE Antennas Wireless Propag. Lett.*, vol. 14, pp. 1638–1641, Aug. 2015.

[13] P. Yang, F. Yan, F. Yang, and T. Dong, "Microstrip phased array in-band RCS reduction with a random element rotation technique," *IEEE Trans. Antennas Propag.*, vol. 64, no. 6, pp. 2513–2518, Jun. 2016.

[14] Y. Jia, Y. Liu, Y. J. Guo, K. Li, and S.-X. Gong, "Broadband polarization rotation reflective surfaces and their application on RCS reduction," *IEEE Trans. Antennas Propag.*, vol. 64, no. 1, pp. 179–188, Jan. 2016.

[15] Y. Jia, Y. Liu, H. Wang, K. Li, and S. Gong, "Low-RCS, high-gain, and wideband mushroom antenna," *IEEE Antennas Wireless Propag. Lett.*, vol. 14, pp. 277–280, 2015.

[16] Y. Liu, K. Li, Y. Jia, Y. Hao, S. Gong, and Y. J. Guo, "Wideband RCS reduction of a slot array antenna using polarization conversion metasurfaces," *IEEE Trans. Antennas Propag.*, vol. 64, no. 1, pp. 326–331, Jan. 2016.

[17] H. L. Zhu, S. W. Cheung, K. L. Chung, and T. I. Yuk, "Linear-to-circular polarization conversion using metasurface," *IEEE Trans. Antennas Propag.*, vol. 61, no. 9, pp. 4615–4623, Sep. 2013.

[18] C. A. Balanis, *Antenna Theory: Analysis and Design*, 3rd ed. Hoboken, NJ, USA: Wiley, 2005.

QIANG CHEN was born in Jiangxi, China. He received the bachelor's and master's degrees from Air Force Engineering University, Xi'an, China, in 2011 and 2013, respectively, where he is currently pursuing the Ph.D. degree in electrical science and technology. His research interests include microwave circuits, antennas, and arrays.

HOU ZHANG received the B.S. degree from Xi'an Electronic and Engineering University, the M.S. degree from the Air Force Missile College, and the Ph.D. degree from Xidian University, all in electromagnetic field and microwave technology. He has published over 150 technical papers and authored/edited six books. He holds six granted/filed patents. His current research interests include planar antennas and EMC. He has been the Session Chair of PIERS and APEMC.

• • •